Chemistry–A European Journal
Research Article
doi.org/10.1002/chem.202402338
Chemistry Europe
European Chemical Societies Publishing
www.chemeurj.org

One-pot Functionalization for the Preparation of Cobaltocene-Modified Redox-Responsive Porous Microparticles

Till Rittner,[a] Jaeshin Kim,[a] Aaron Haben,[b] Ralf Kautenburger,[b] Oliver Janka,[b] Jungtae Kim,[c] and Markus Gallei*[a, d]

This paper is dedicated to Ian Manners and his inspiring work on metallopolymers.

Porous organic cobaltocenium-containing particles are scarce in literature but highly interesting for their electrochemical properties and reusability in, for example, catalysis or magnetic systems. In this work, we present a scalable one-pot strategy to introduce tailorable amounts of cobaltocenium on a porous substrate, adjusting the electrochemical switching capability. For this purpose, 3-(triethoxysilyl)propan-1-amine (APTES) and ethynyl cobaltocenium hexafluorophosphate is used as functionalization agents for in-situ catalyst-free hydroamination, followed by silane condensation at the particles' surface. Functionalized particles are characterized by attenuated total reflection infrared spectroscopy (ATR-IR), thermogravimetric analysis (TGA), laser scanning confocal microscopy (LSCM), scanning electron microscopy (SEM), energy dispersive X-ray spectroscopy (EDS), inductively coupled plasma mass spectrometry (ICP-MS), powder X-ray diffraction (PXRD) and cyclic voltammetry (CV) showing excellent control over the degree of functionalization, i.e., the added cobaltocenium reagents. The electrochemical stability and good addressability while preserving the porous structure are shown. By utilizing higher amounts of APTES, the overall cobaltocenium amount can be reduced in favor of additional amine groups, strongly affecting the electrochemical behavior, making this functionalization strategy a good platform for metallopolymer immobilization and tailored functionalization. Additionally, thermal treatment of the synthesized metallopolymer microparticles paves the way to magnetic properties with tailorable microporous architectures for end-of-life and upcycling aspects.

Introduction

Due to the ever-growing complexity of modern materials, metallocenes have recently attracted increasing attention.[1] This class of metal-organic compounds combines key features from both aspects of chemistry: (i) On the one hand, the coordinated metal center of the metallocene can be electronically addressed and change the oxidation state upon applying a voltage.[2] (ii) On the other hand, these complexes are very versatile for functionalization due to their organic ligands, reactivity, and addressability, which can be altered.[3] One of the most prominent and well-investigated metallocenes is ferrocene.[4] Here, the central iron atom is coordinated by two cyclopentadiene ligands in a "sandwich"-like structure and can switch from the neutral Fe^{II} to the cationic Fe^{III} state upon electrochemical oxidation.[5] This switching process is highly reversible over numerous cycles, and ferrocene is therefore used in electrochemical analysis such as cyclic voltammetry (CV) as an internal standard or calibration agent. Besides its use in electrochemistry, ferrocene, and its derivatives may also be used as fuel enhancers and octane reduction agents in the modern petrol industry.[6] In the field of advanced materials, the fixation of ferrocene on a surface can be useful.[7] Here, two different strategies are commonly applied: (i) fixation via functionalization of the target material with modified ferrocene compounds[8] and (ii) the tailored design of ferrocene-containing polymers.[9–11] In the first approach, ferrocene is modified so moieties near the ferrocene unit can immobilize the compounds on a target surface. For the second approach, the ferrocene is added to a polymer structure by postmodification of the reactive polymer backbone, or a polymerizable ferrocene-containing monomer is utilized. Ian Manners pioneered ferrocene-containing polymers in this regard by introducing metallocenophanes as a building block.[12] A large class of main-chain metallopolymers was established by ring-opening-polymerization (ROMP) of these ring-strained metallocenes. Com-

[a] T. Rittner, J. Kim, M. Gallei
Polymer Chemistry, Saarland University, Campus C4 2, 66123 Saarbrücken, Germany
E-mail: markus.gallei@uni-saarland.de
[b] A. Haben, R. Kautenburger, O. Janka
Inorganic Solid State Chemistry, Saarland University, Campus C4 1, 66123 Saarbrücken, Germany
[c] J. Kim
Korean Institute of Science and Technology, Campus E 7 1, 66123 Saarbrücken, Germany
[d] M. Gallei
Saarene, Saarland Center for Energy Materials and Sustainability, Campus C4 2, 66123 Saarbrücken, Germany

Supporting information for this article is available on the WWW under https://doi.org/10.1002/chem.202402338

pared to ferrocene-based molecules, ferrocene-containing polymers provide unique features, and they have been used for control of the surface wettability,[13] in catalysis,[14] ion sensing,[15] battery applications,[16–17] or as a precursor for ceramic material.[18] Moreover, ferrocene-containing polymers' switching capability can be used to prepare redox-responsive opal films with switchable structural colors,[19–22] membrane gating,[23–25] and many other applications that have been reviewed recently.[9,26–27] One downside of ferrocene is that the less stable cationic Fe^{III} state is prone to reduce to the favored neutral Fe^{II} form. Here, the ionic state could be utilized for a vast range of applications but is limited to specific conditions where it is stable.[28] By diverting from iron to cobalt as central atoms for the metallocene, an additional electron is introduced to the complex. The now-established cobaltocenium complex is isoelectronic to ferrocene but favored in the permanently charged state. As a result, the neutral cobaltocene complex oxidizes like alkali metals readily with an available reductant to the ionic species.[29] It is therefore utilized in organic synthesis as one electron-reducing agent,[30] for the synthesis of new carbon material,[31] as a precatalyst,[32] and in the electrochemical analysis as standard at lower voltages than ferrocene.[33] The cobaltocene salt is very robust and withstands a vast range of reactions and conditions ferrocene cannot tolerate. On the contrary, it is more challenging to functionalize cobaltocenium to a desired valuable structure for immobilization onto different surfaces.

Nevertheless, cobaltocenium can be used in various materials like polymers and hydrogels.[34] For example, electrochromic polymers could be synthesized by Gu et al.[35] Recently, Feuerstein et al. prepared water-soluble main-chain cobaltocenium polymers with interesting electric and ion exchange properties.[36] Antifouling and antimicrobial properties were reported for cobaltocenium-containing hydrogels.[37–38] However, compared to ferrocene, examples where redox-active cobaltocenium-functionalized materials can be electrochemically addressed are underrepresented in the literature. Functionalization on highly porous substrates is attractive due to its feasibility for surface-based catalytic and analytic applications.[39] Compared to the rather lab-intense approaches, a practical pathway for surface-functionalization strategies is needed.

This work presents a convenient approach to introduce cobaltocenium moieties to porous microparticle surfaces via a one-pot reaction. For this purpose, the 3-(triethoxysilyl)propane-1-amine (APTES) motive is used in a catalyst-free coupling reaction. By this strategy, the amount of cobaltocenium on the particle can be introduced in a controlled fashion. The resulting particles are characterized regarding the surface functionalization using attenuated total reflection infrared spectroscopy (ATR-IR), scanning electron microscopy (SEM), and energy-dispersive X-ray spectroscopy (EDS), and the cobaltocenium content by thermogravimetric analysis (TGA) and inductively coupled plasma mass spectrometry (ICP-MS). For further applications, the electrochemical addressability is analyzed by cyclic voltammetry (CV), and the preceramic material's feasibility is shown.

Results and Discussion

Cobaltocenium and Precursor Synthesis

First, a scalable synthesis procedure was developed compared to literature-known strategies[40] for investigating and functionalizing redox-responsive materials with cobaltocenium. For this purpose, $Cp_2Co\ PF_6$ **4** was synthesized in a one-pot approach, starting from cyclopentadiene **1** via sodium cyclopentadiene **2** to cobaltocene **3**, followed by oxidation and anion exchange. The synthesis is given in Scheme 1.

For the initial retro Diels-Alder reaction, a solvent with a high boiling point and stability in the presence of sodium was used, and anisole was found to be suitable. At the boiling point of anisole (154 °C), the reaction **1** to cyclopentadiene and direct conversion to sodium cyclopentadiene (NaCp) **2** was possible. Here, **2** possessed only limited solubility in anisole, and after the addition of a cobalt salt and workup, **4** was acquired with a low yield of 33%. Hence, tetrahydrofuran (THF) was added as a solubilizer (cf. experimental section). The highest conversions were achieved using a volume ratio of 1 to 2 of anisole to THF. In the next step, cobalt salts and oxidation methods were further investigated. Anhydrous cobalt bromide ($CoBr_2$) followed by oxidation in water in the presence of air showed the best results concerning the yield and purity of the product. In addition, potassium hexafluorophosphate (KPF_6) proved advantageous in comparison to dangerous hexafluorophosphate acid. For example, the herein-developed procedure could acquire 52 g of the desired cobaltocenium PF_6 **4** with a 72% yield.

As presented in Scheme 1b), ethynyl cobaltocenium **6** was synthesized in a two-step reaction by a modified procedure from the literature.[41] For this purpose, TMS-acetylene was subjected to a nucleophilic addition reaction, followed by hydride abstraction and anion exchange, to obtain the TMS-protected ethynyl cobaltocenium **5**. After desilylation of the acetylene group with potassium bifluoride (KHF_2), **6** was obtained in an overall yield of 75%. As a note, the ^{1}H-NMR spectrum (Figure S3) indicated the presence of 7% of residual **4**, which is a typical byproduct of the deprotection and is known to literature.[41] No negative influence on further reaction steps was found for the following reactions, and the residual **4** could be removed via subsequent workup procedures. Finally, the functionalization agent APTES-cobaltocenium **7** was synthesized in analogy to literature in acetonitrile (Scheme 1c).[42] The reaction proceeded rapidly, and the quantitative conversion of **6** to the red product **7** could be identified from the corresponding ^{1}H NMR spectrum (Figure S4). In our efforts to synthesize a redox-responsive material, it was crucial to characterize the oxidation-reduction profile of the functionalization agent. For this purpose, cyclic voltammetry of **7** was performed in acetonitrile with ferrocene (Fc) as the internal standard. In more detail, a platinum working and counter electrode and an Ag/AgCl reference electrode were used. As can be concluded from the obtained electrochemical results in Figure 2d, a reversible electron transfer from Co^{III} to Co^{II} could be found at $E_{1/2} = -1.56$ V (vs Fc/Fc^+) and $\Delta E_p = 0.035$ V. Next to the primary signal, several smaller signals can be found in the

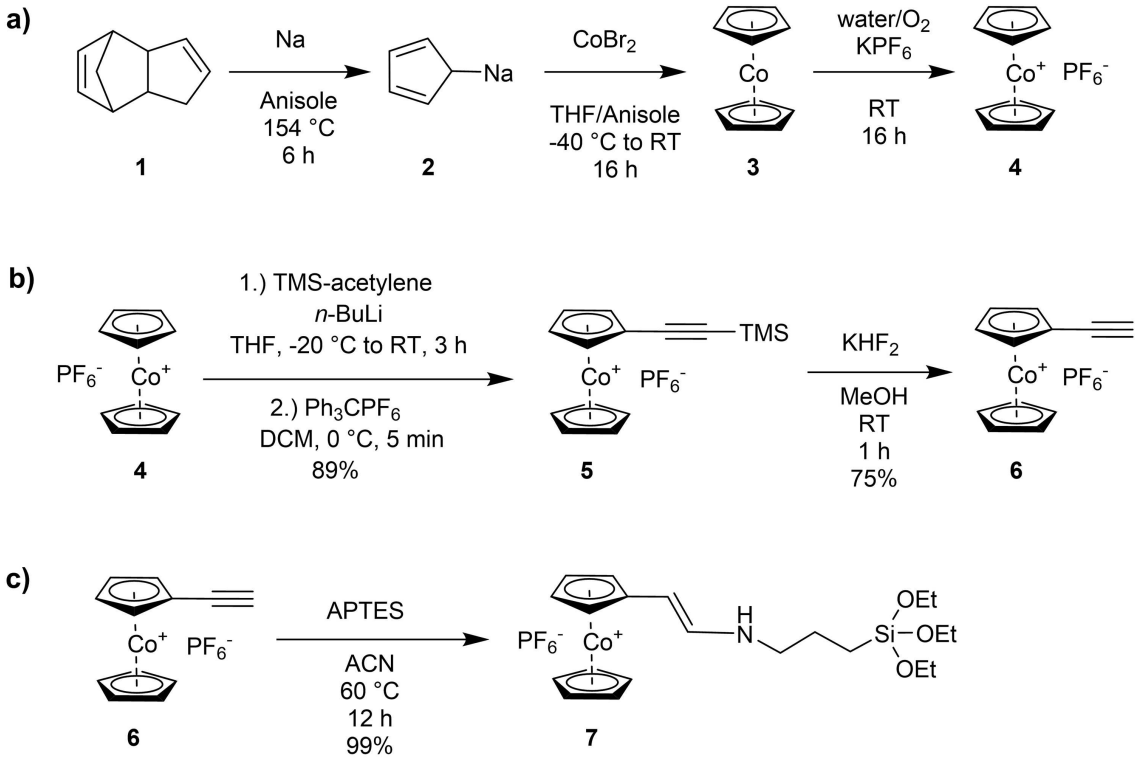

Scheme 1. a) One-pot synthesis of cobaltocenium PF_6 **4** starting from dicyclopentadiene **1** and sodium in anisole to form sodium cyclopentadiene **2**. Cobaltocene **3** formation was accomplished by $CoBr_2$ addition and oxidation to **4** in an overall yield of 71.5%. **b)** Synthesis of ethynyl cobaltocenium PF_6 **6** starting with a nucleophilic addition and hydride abstraction leading to **5** followed by desilylation of ethynyl-TMS to yield **6**. **c)** Formation of the 3-(aminopropyl) trimethylsilyl (APTES)-cobaltocenium derivative **7** via hydroamination addition starting from **6**.

−1.4 V to −1.2 V region. These were attributed to the conjugation of the cobaltocenium to the amine linker. Additionally, scanning rate-dependent measurements (Figure S10) further confirmed the reversible redox-active nature of this compound, thus qualifying this component for the subsequent functionalization and investigations of redox-responsive particle systems, as given in the following sections.

Particle Functionalization

A substrate with high stability and porosity, which can be easily separated using conventional industrial processes, was used as a template for functionalization. Hydroxy-rich polystyrene-polydivinylbenzene (PSDVB) particles[43] were ideal substrates. Such particles possess good stability and accessibility to the porous structure and are known to be useful for catalysis systems and templates for other applications.[44–45] Furthermore, particles of several μm in size can be easily removed from the reaction medium by centrifugation or filtration. The functionalization with the redox-responsive moieties was performed via a sol-gel condensation reaction of the siloxane group. This way, a higher degree of functionalization is obtained due to forming a condensate siloxane network rather than a monolayer. This behavior is well-known in the literature and is widely used for APTES and similar mono- and multi-functional siloxanes.[13,46–52] In our case, two different strategies were followed, which are displayed in Scheme 2: to verify the functionalization capability, in the first strategy (**a**+**b**), APTES was attached, the particles were purified, and in a later step, cobaltocenium was introduced. In a second approach (**c**), the cobaltocenium motive was attached directly via a one-pot procedure. In the following, both pathways are described and discussed for comparison.

To verify the covalent immobilization of the APTES-derived cobaltocenium motive **7**, APTES itself was first condensed to the particle surface Scheme 2a. A standard procedure in toluene with triethylamine as an auxiliary base was used.[53] In the second step, ethynyl cobaltocenium **6** was attached in acetonitrile. ATR-IR spectroscopy was used to monitor the synthesis for initial tests, and the resulting spectra are shown in Figure 1a. As can be concluded from these results, APTES-functionalized particles (red) showed a significant resonance for $\nu_{(C\text{-}N)}$ in the 1150–1000 cm^{-1} region (violet signals), indicating the success of APTES functionalization (black). After functionalization with **6**, the analyzed particles display additional signals at 839 cm^{-1} (orange, $\nu_{(PF6)}$) and 559 cm^{-1} (red, $\nu_{(cyclopentadienyl)}$), which could be attributed to newly introduced cobaltocene motives according to the literature.[42] For further comparison, APTES-cobaltocenium **7** (blue) is shown additionally. As shown in the photograph in Figure S5, the particles featured a bright red color after functionalization compared to the colorless APTES-functionalized particles.

To conclude, we could show that this functionalization route successfully immobilized the redox-active cobaltocenium

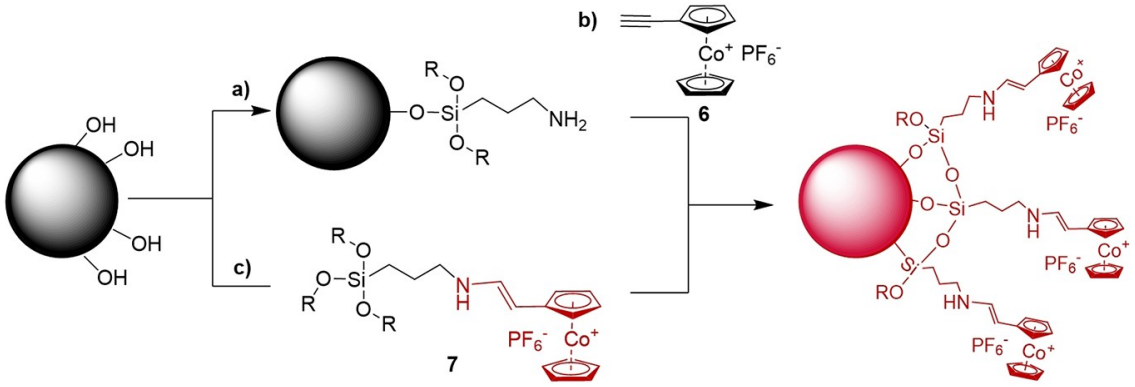

Scheme 2. Synthesis of cobaltocenium-functionalized microparticles via two different approaches: First, by two-step functionalization with (**a**) hydroxy-rich PSDVB, 3-(aminopropyl)triethylsiloxane (APTES) and triethylamine in toluene at 85 °C for 48 h; and (**b**): APTES-functionalized particles and ethynyl cobaltocenium PF_6 (**6**) in acetonitrile at 75 °C for 2.5 d. Second by one-pot functionalization-reaction (**c**): hydroxy-rich PSDVB with functionalization agent **7** in acetonitrile at 80 °C for 4 d.

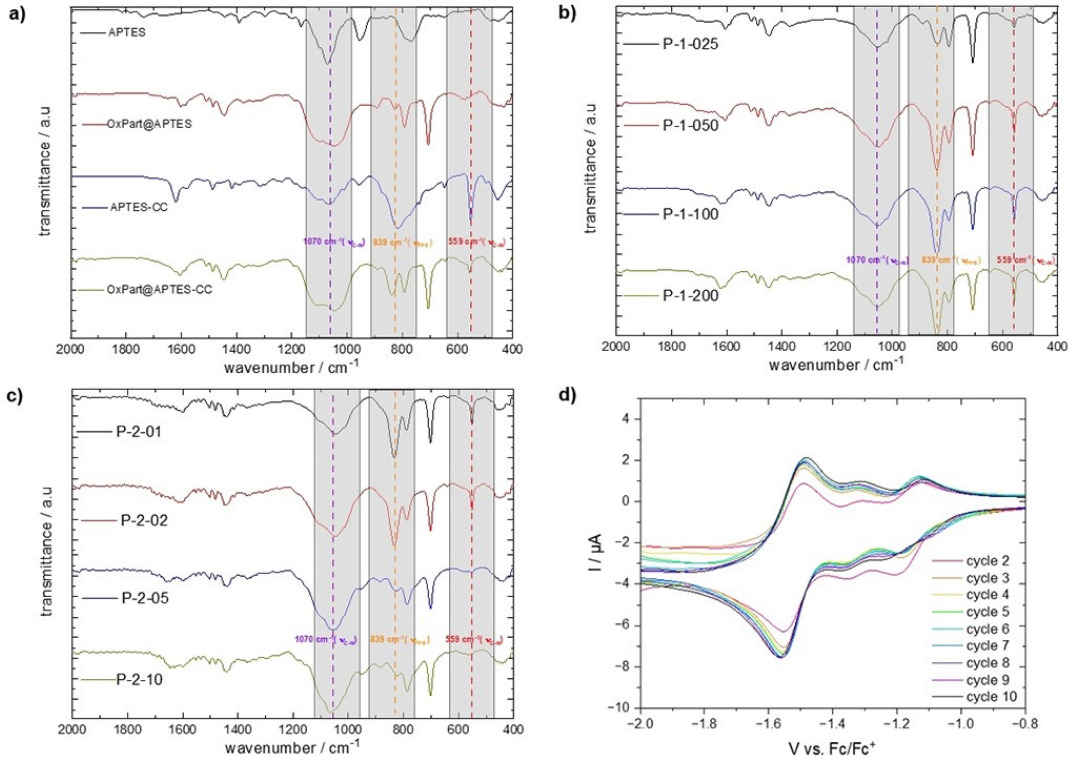

Figure 1. ATR-IR spectra of synthesized microparticles and CV data of **7**; **a)**: ATR-IR spectra of initial two-step functionalization by functionalization with 3-(aminopropyl)triethylsiloxane (APTES) to APTES functionalized PSDVB particles (OxPart@APTES) and particles after cobaltocenium functionalization (OxPart@APTES-CC), additionally compared to later used functionalization agent **7** (APTES-CC); **b)**: **P-1** series with an increasing amount of functionalization agent (P-1-XXX wt%) per 100 mg of particles used **c)**: **P-2** series with an increasing amount of APTES equivalents (P-2-XX eq.) compared to cobaltocenium, **d)**: CV investigation of **7** in acetonitrile with 0.1 M $TBAPF_6$ at a scan rate of 50 mV s^{-1}, Pt working, and Ag/AgCl as a reference electrode.

moieties on the particles' surface. Different degrees of cobaltocenium modifications could be obtained by varying the amount of APTES at the particle surface. However, one particular downside of this strategy is the extensive purification necessary after each functionalization step. Due to the porous architecture and resulting high surface area, purification in a range of organic solvents and multiple repetitions were necessary to avoid the leaching of adsorbed unreacted functionalization agents. These would otherwise interfere with the following functionalization reaction steps and affect the electrochemical addressability. Furthermore, due to the ionic character of the ethynyl cobaltocenium and the overall large surface of the porous particle, a quantitative conversion of the condensed APTES could not be guaranteed. Therefore, to further facilitate

and improve the functionalization process and to eliminate one of the required washing steps in between the reactions, a second synthesis route was developed, as described in the following. In a one-pot approach displayed in Scheme 2c, the APTES-cobaltocenium complex **7** was first formed in acetonitrile in the reactor. The solid microparticles were added in the next step, and the resulting suspension was stirred at 80 °C for 4 days. This strategy was more straightforward, as no additional auxiliary base was needed for the surface modification. After successful purification, no leaching or detaching of the cobaltocenium motive was found after storing the particles in acetonitrile for an extended period, and it could be ensured that each condensed APTES unit also contained the desired cobaltocenium unit. Furthermore, by additional equivalents of APTES, the introduced amine content could be tailored in a more controlled fashion. Therefore, two distinct series of experiments were conducted to tailor the surface properties further. In the first set, the overall amount of APTES-cobaltocenium complex was increased (**P-1**), and in the second, the ratio of APTES to cobaltocenium was varied (**P-2**). To further distinguish between the different samples in a series, and since the formed complex **7** was not investigated in detail for every reaction, the experimental values were added to form the final name. Here, the amount of used ethynyl cobaltocenium per 100 mg of starting material is given in weight percent like P-1-XXX (wt%), resulting in **P-1-025 (25 wt%)** to **P-1-200 (200 wt%)** and the APTES equivalents compared to cobaltocenium used, are shown like P-2-XX (eq.) resulting in **P-2-01** to **P-2-10**. To assess the ceramic potential via calcination and to confirm the scalability of the reaction, the gram-scale synthesis of **P-3** was performed. Synthesized particles and reaction parameters are compiled in Table 1, while the analyses of the resulting microparticles are given in the following sections.

Analyses of Microparticles Featuring Redox-Active-Moieties

To gain insights into the amount of grafted redox-active species and the microparticles' surface properties, the resulting particles were first qualitatively analyzed by attenuated total reflection infrared (ATR-IR) spectroscopy. As shown in Figure 1b, the amount of functionalization reagent used correlates with the degree of functionalization of the resulting particles after synthesis. This dependency could be concluded from the general increase in signal intensity for the resonances at 839 cm^{-1} ($\nu_{(PF6)}$) and 559 cm^{-1} ($\nu_{(CP)}$).[42] The ATR-IR data revealed increased APTES-cobaltocenium resonances up to sample **P-1-100**. The difference in intensity to **P-1-200** turned out to be marginal, indicating a similar composition and, therefore, a plateau for the degree of functionalization in the form of saturation. It is proposed that at this point, the suitable surface for functionalization was covered to a possible maximum due to steric hindrance of attached moieties or the cobaltocenium-induced charge density limits further addition. On the other hand, by increasing the APTES content, less cobaltocenium complex was incorporated. This can be shown by comparing the APTES to cobaltocenium signals in Figure 1c. At ten equivalents per cobaltocenium unit (**P-2-10**), respective signals were only slightly visible, indicating a low cobaltocenium content. Due to the lack of calibration for cobaltocenium and APTES derivatives, and the porous structure of the particle, the IR data could not solely be used for quantification. In order to make a better statement about the degree of functionalization, the IR data had to be expanded by further characterization methods.

Another suitable analytical tool to verify the content of a metal-containing material is thermogravimetric analysis (TGA). Normally, solid carbon and gasses like oxygen and carbon dioxide (CO_2) are mainly formed for the non-functionalized particles. By introducing silica and cobalt to the carbon scaffold, both hetero atoms form ceramic materials during thermal treatment. Therefore, further insights into the particle surface and the overall composition can be made by assessing the residual weight after burning the synthesized particles. This is a suitable method for verifying the cobalt content of cobalt-containing organic compounds and polymers.[34] The standard procedure was thermal treatment in a (i) nitrogen atmosphere (ii) up to 590 °C for all investigated functionalized microparticles. For this purpose, both particle series were compared and graphs and the residual weights are presented in Figure 2. Here, a substantial mass decrease above 350 °C could be found for all microparticles, which was attributed to the disintegration

Table 1. Overview of synthesized particles and parameters.

Sample	Ethynyl Cobaltocenium wt%	APTES mg	APTES equivalents	Ox_Particles mg
P-1-025	25	15.45	1	100
P-1-050	50	30.91	1	100
P-1-100	100	61.82	1	100
P-1-200	200	123.63	1	100
P-2-01	50	30.91	1	100
P-2-02	50	61.82	2	100
P-2-05	50	154.54	5	100
P-210	50	309.08	10	100
P-3	100	3710	1	6000

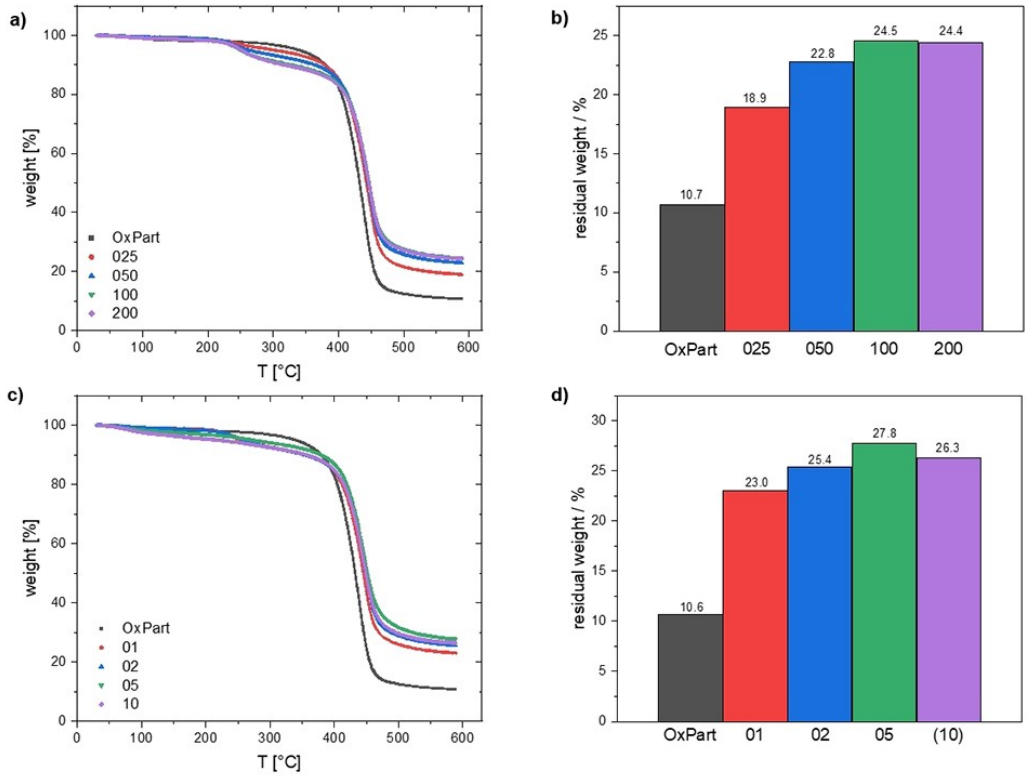

Figure 2. TGA graph of synthesized particles in nitrogen gas from 30 to 590 °C with a heating rate of 10 K min^{-1}. **a)**: TGA of **P-1**, **b)**: residual mass of **P-1** **c)**: TGA of **P-2** **d)**: residual mass of **P-2**.

of the carbon structure. Additionally, a different deterioration over 250 °C could be observed. This degradation step increased with increasing cobaltocenium content, indicating an additional degradation process introduced by the functional group. As indicated by the IR data, a stepwise increase in residual mass was found in the **P-1** series, revealing a plateau at approximately 24.5 wt% (Figure 2b). Compared to the relatively sharp mass decrease for the cobaltocenium, a gradual decrease rather than a step could be found for the APTES series in Figure 2c. This gradual decrease was attributed to the siloxane network formation, where additional condensation reactions could occur at elevated temperatures with non-reacted ethoxy silane moieties.[54–56] A stepwise increase of the residual mass with increasing APTES equivalents up to **P-2-05** was found. The residual weight was also higher compared to **P-1-100**, indicating better incorporation of silica or self-condensation of APTES at the particle surface. Here, APTES was considered to be smaller concerning size and without the occurrence of an osmotic pressure, as for the charged cobaltocenium derivative, additional condensation is more likely.

To confirm that the cobaltocenium-modified particles were not damaged during the functionalization and that no undesired particle deformation occurred, laser scanning confocal microscopy (LSCM) studies were performed (Figure 3). Here, sample **P-1-050** is shown exemplarily, while further images can be found in the Supporting Information section (Figure S6). As can be concluded from these images, the microparticles appeared unharmed by the herein-described synthesis strategies. For the laser intensity (**a**) and color mode (**b**) presented in Figure 3, the particles appeared round-shaped, featuring an even size distribution of 5.16 ± 0.22 µm (Table S1). The porous structure could be observed via 3D height imaging (Figure 3c + d) with a homogeneous distribution.

Scanning electron microscopy (SEM) and energy-dispersive X-ray spectroscopy (EDS) were performed to investigate further the particle structures, porosity, and amount of cobalt functionalization. From the corresponding photographs, the porous structure and particle integrity could again be verified (Figure S7 + S8). In addition, the particle sizes were measured to be in a range of 4.3 ± 0.3 µm (**P-1-025**) for the lowest to 4.5 ± 0.2 µm (**P-2-10**) for the highest degree of functionalization. A detailed list of the respecting sizes, errors, and derivation from the non-functionalized microparticles can be found in Table S2. Additionally, Figure 4d presents the size difference in percent to the original particles. An almost linear increase in particle size with modification with each series could be found. As mentioned, the P-1 series was slightly smaller than the P-2 series due to a more minor degree of functionalization.

EDS of all particles were measured, and all samples contained homogeneously distributed cobalt. In Figure 4, exemplary measurements of **P-1-200** are shown as plane image (**a**), with silicon (**b**) and cobalt (**c**) mapping. The values found for

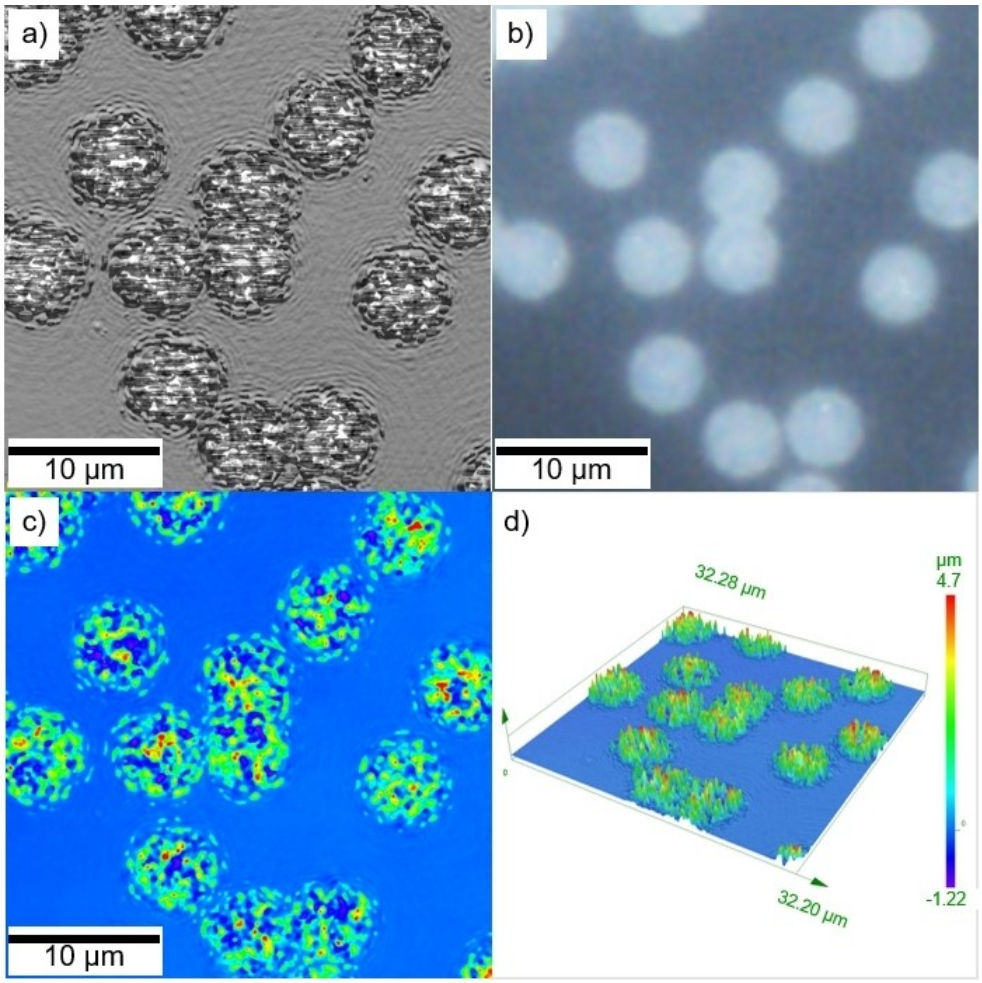

Figure 3. LSCM data of synthesized particles **P-1-50**. **a)** Laser intensity mode, **b)** color mode, **c)** height mode, **d)** 3D height plot.

cobalt and silicon directly correlated with the respective degree of microparticle functionalization. However, the amount of cobalt could only be roughly estimated via EDS. Still, a trend was already observable, consistent with previously discussed results on the amount of functionalization (Table 2): a steady increase with a higher degree of cobaltocenium functionalization was observed. Again, the difference between the two most significant degrees of functionalization was only marginal, indicating a saturation of the degree of modification. In contrast, a decline in cobalt intensity with higher APTES content was found. However, as EDS in combination with the SEM was not specifically calibrated, only rough values for cobalt at the

Table 2. Overview of cobalt determination by EDS and ICP-MS.

Sample	EDS wt%	ΔEDS wt%	ICP-MS µg[a]	ΔICP-MS µg[a]
P-1-025	4.77	0.60	37.99	0.04
P-1-050	9.91	2.24	75.69	0.05
P-1-100	12.26	1.53	111.92	0.03
P-1-200	14.47	0.91	132.29	0.01
P-2-01	8.99	1.01	83.18	0.02
P-2-02	7.13	0.17	89.22	0.07
P-2-05	2.91	0.32	45.58	0.05
P-2-10	2.86	0.09	40.13	0.04

[a] Value per 10 mg of analyzed particles.

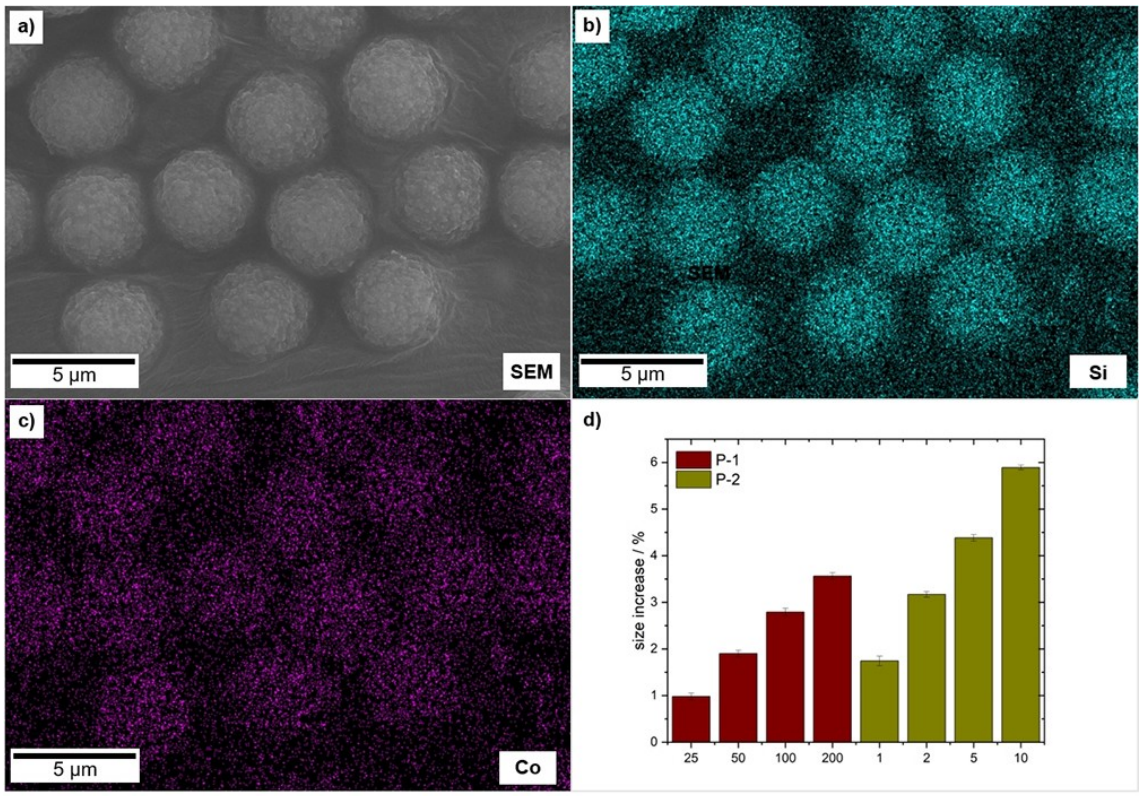

Figure 4. SEM photographs and EDS data of synthesized particles **P-1-200**. **a)**: SEM image, **b)**: silicon mapping, **c)**: cobalt mapping, **d)**: size difference of functionalized particles compared to the pristine particles (given in percent) with increasing amounts of cobaltocenium (P1, red) (25 to 200 wt% with respect to the particle mass) and increasing equivalents of APTES compared to cobaltocenium (P2, yellow) for the functionalization.

particles' surface could be obtained. Therefore, inductively coupled plasma mass spectrometry (ICP-MS) was additionally used for the cobalt quantification.

For ICP-MS measurements, digestion of the functionalized particles with aqua regia was performed first. The resulting solution was used to analyze the cobalt amount. In Table 2, the data determined by ICP-MS and EDS were directly compared. The **P-1** EDS and ICP-MS values results revealed a similar trend with saturation at around 13.23 µg mg^{-1} or 1.32 wt% cobalt. In contrast, the **P-2** series showed more cobalt at higher APTES equivalents than expected by EDS and ATR-IR spectroscopy. It is presumed that the condensation rate of the silane components and the network's development strongly differ between the modified and unmodified APTES. We propose that modified APTES **7** is preferably condensed to the particle surface due to favorable (ionic) interactions with the oxidized particle. Unmodified APTES reacts later on to form the network and overgrows the cobaltocene derivative, making it less addressable for EDS and ATR-IR spectroscopy.

At the end of the product lifetime, calcination is generally a great way to upcycle used catalytic material to repurpose, extend usability, and reduce costs.[57] As a comparison, similar approaches are performed extensively for cobalt-containing lithium-ion battery cathodes.[58] Cobalt oxide-containing nanostructures synthesized by calcination are attractive for energy storage solutions and other applications. Furthermore, calcination is known in the literature for similar functionalized porous ferrocene-containing particles and cobaltocenium-containing polymers.[44] For this reason, the calcination of the synthesized cobaltocenium-containing particles was investigated. Here, particles of **P-3** were treated under synthetic air (**P-3-ox**) or nitrogen atmosphere (**P-3-N_2-800**) up to 800 °C. A significant difference concerning the residual weight could be found. While calcination in nitrogen resulted in a residual weight of 21 wt%, microparticles in synthetic air resulted only in 7% due to the oxidative environment leading to carbon removal as CO_2. In addition, SEM analysis of the residual ceramic material (Figure 5) showed a significant decrease in size from an initial 4.2 ± 0.2 µm to 1.2 ± 0.1 µm in oxygen and 2.1 ± 0.1 µm in nitrogen. Furthermore, the porous particle structure was still present for all thermally treated calcinated samples. When particles were exposed to an ordinary magnet, **P-3-N_2-800** revealed macroscopic magnetic properties (Figure 5g). The presence of elemental cobalt was the reason for the magnetic behavior. To verify this assumption, another calcination protocol up to 970 °C was conducted (**P-3-N_2-970**), where cobalt metal is known to react with carbon sources.[59–60] As presented in Figure 6h, the calcination product was not magnetic anymore. The respective calcination products were investigated further using powder X-ray diffraction (PXRD) and EDS. Additional cobalt metal domain size reduction from 10 ± 2 nm to 3 ± 2 nm was found at higher calcination temperatures in

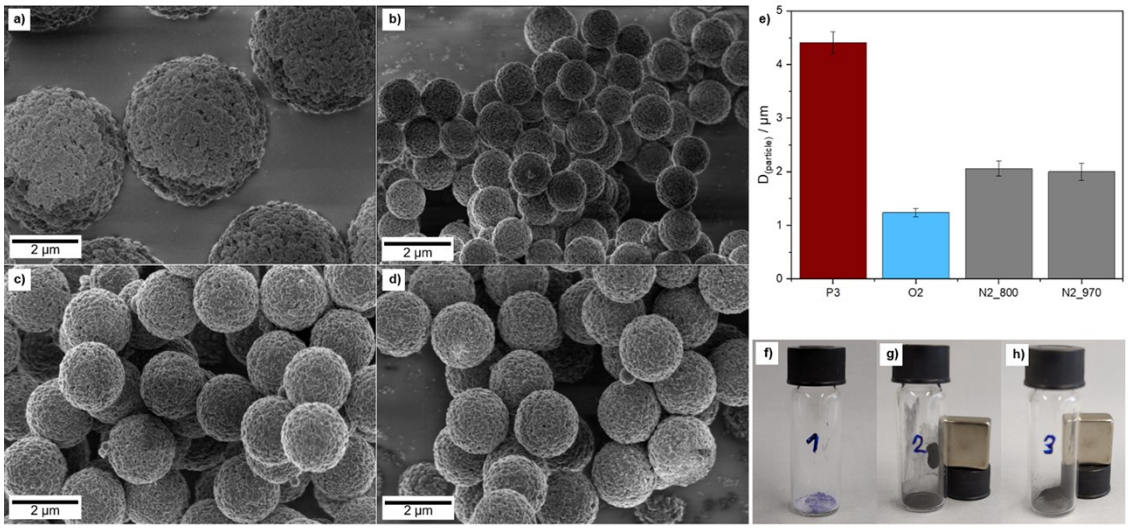

Figure 5. SEM images of particles before (**P3**) and after calcination in synthetic air (O_2) or nitrogen (N_2) atmosphere with a heating rate of 10 K min^{-1} and final temperatures of 800 to 970 °C: **a) P-3** starting material. **b) P-3-ox**. **c) P-3-N_2-800**. **d) P-3-N_2-970**; **e)** particle size comparison before and after different calcination procedures. Appearance and magnetic properties are presented for **f) P-3-ox** (purple, non-magnetic). **g) P-3-N_2-800** (black, magnetic). **h) P-3-N_2-970** (black, non-magnetic)

nitrogen atmosphere. This further supported the proposed magnetic properties of the obtained material. No other significant change in composition regarding the nitrogen samples was observed (Table S4). Hence, the material's magnetic properties could be altered without a substantial change in composition. Moreover, the calcination of the synthesized material displayed overall low crystallinity and a complex composition. Additional information regarding ceramic composition analysis via EDS and PXRD can be found in the supporting information. To conclude, application regarding energy materials is limited due to the overall low ceramic yields, but considerable for end-of-life or upcycling of used catalytic material featuring interesting magnetic properties.

Finally, CV measurements of the functionalized microparticles were performed to address the redox-responsiveness of herein-investigated microparticle systems. An overview is given in Figure 6. Since the particles cannot form stable dispersions, the measurements in dispersion were difficult. In literature, this problem was described for ferrocene-containing microparticles.[44–45] To still address the redox-responsiveness of the functionalized microparticles, the particles were deposited on the electrode surface. Nevertheless, stability and adhesion on the electrode surface of the coatings during measurement were difficult to achieve. The switching potentials were set at −2.5 V and −0.5 V, and acetonitrile was chosen as a stable solvent, having a wide potential window for constant CV analysis without electrolysis. All samples generally featured a reversible or quasi-reversible behavior with an $E_{1/2} = -1.428 \pm 0.027$ V and an $\Delta E_p = 0.077 \pm 0.018$ V.[61] An overview of the CV data is given in Table S3. Due to the high sensibility towards chemical interactions, different environments, and reduced diffusion speed, the energy transfer turned out to be slower, and the signal decreased while slightly shifting to higher voltages compared to functionalizing agent **7**. As for **7**, an additional oxidation peak at -1.065 ± 0.029 V can be found in some samples, attributed to the amine conjugated with the cobaltocenium. Due to the challenging preparation and the high sensitivity towards chemical and solvent interactions, a direct comparison of the obtained data must be considered with caution. Generally, by increasing the amount of cobaltocenium grafted onto the particle, the redox-addressability increased. For **P-1-200**, in addition to regular CV measurements, the electrochemical stability was investigated, showing a slight decrease in signal intensity but overall stability and reversibility over 50 cycles (Figure 6d). As expected for the **P-2** samples, by increasing the APTES content on the particle surface, the addressability of the cobaltocenium decreased, and the dominance of the electric interaction of the amine (linker) increased. Multiple measuring cycles were measurable for all cases with only slight deviation, displaying reversible redox activity. It was, therefore, possible to control the material's electric properties by tailoring the cobalt and the amine amount on the particle surface.

Conclusions

Due to their electrochemical properties, highly porous organic cobaltocenium-containing particles are sought after for reusability in heterogenic catalysis systems. On the other hand, literature on synthesizing these materials and the commercial availability of the cobaltocene starting material is limited. We have shown the large-scale one-pot synthesis of cobaltocenium hexafluorophosphate starting from dicyclopentadiene and sodium in an overall yield of 72%. Furthermore, we presented the functionalization of porous oxidized polystyrene-based particles to cobaltocenium-containing material in two separate ways: First, by functionalizing with 3-(triethoxysilyl) propane-1-

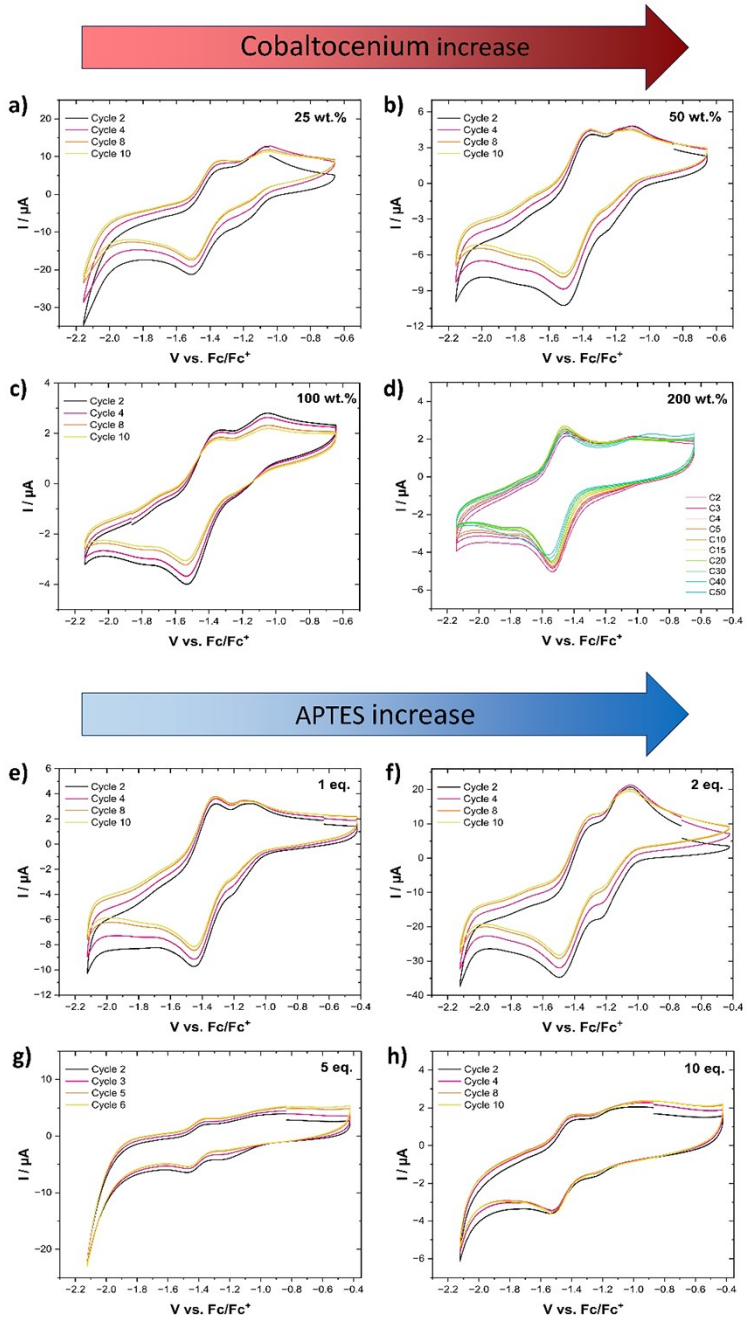

Figure 6. CV investigation of particles in acetonitrile with 0.1 M $TBAPF_6$ at a scan rate of 200 $mV\,s^{-1}$, Pt working, and Ag/AgCl reference electrode with increasing cobaltocenium (P-1) or APTES (P-2) amounts. **a) P-1-025**. **b) P-1-050**. **c) P-1-0100**. **d)** 50 cycles of **P-1-200**; **e) P-2-01**. **f) P-2-02**. **g) P-2-05**. **h) P-2-10**.

amine (APTES) and introducing cobaltocenium in a second step. On the other hand, in a one-pot approach, an APTES-cobaltocenium reagent was used directly. By this method, tunable amounts of cobaltocenium as well as APTES could be introduced to the surface and verified via attenuated total reflection infrared spectroscopy (ATR-IR), thermogravimetric analyses (TGA), and inductively coupled plasma mass spectrometry measurements (ICP-MS), in addition. Laser scanning confocal microscopy (LSCM) and scanning electron microscopy (SEM) confirmed the functionalization of the particle surface without losing the desired porosity. Moreover, the calcination of the synthesized material displayed overall low crystallinity and a complex composition. Magnetic properties could be tailored by varying the calcination protocol. Lastly, synthesized particles were characterized by cyclic voltammetry (CV), showing redox-addressability, reversibility, and stability over high cycling numbers. It was found that by introducing an increasing amount of cobaltocenium or amine, the electrochemical profile can be tailored, which is promising for future applications.

Experimental Section

General

All solvents and reagents were purchased from Alfa Aesar (Haverhill, MA, USA), Sigma-Aldrich (St. Louis, MA, USA), Fisher Scientific (Hampton, NH, USA), ABCR (Karlsruhe, Germany) and used as received unless otherwise stated. Deuterated solvents were purchased from Deutero (Germany). PSDVB particles were donated by Metrohm. Proton nuclear magnetic resonance (^{1}H-NMR) spectra were recorded on a Bruker Avance II 500 spectrometer with a 9.4 T Ultrashield Plus Magnet and a BBFO probe and referenced using the solvent signals. For processing and evaluation of the spectra, MestReNova 14.2.0 was used. Infrared (IR) spectra were collected on a BRUKER ALPHA II FT-IR setup in attenuated total reflection mode (ATR) with spectrum output in transmittance. All spectra were processed with OPUS 8.5 (SP1) software (baseline correction) and Origin2020b (normalized). Thermogravimetric analyses (TGA) were carried out on a Netzsch TG 209 F1 Libra with a heating rate of 10 K min^{-1} and synthetic air as protective and nitrogen as purge gas with a flow rate of 20 mL min^{-1} each. For evaluation, Netzsch Proteus Thermal Analysis 8.0.1 was used. Laser scanning confocal microscopy (LSCM) images were taken from Olympus LEXT OLS5100 3D laser scanning confocal microscope. A 405 nm laser and visible light with a 0.95NA high-performance objective lens were used. A micro x-y scanner, motorized stage, and autofocusing features provide a digital 3D profile with 0.12 μm lateral resolution in non-contact measurement. Images were obtained using a 50×0.95NA objective lens and dual DIC (differential interference contrast) laser with high dynamic color range (HDR) exposure controls. Multiple z-directional images were taken with 120 nm height shifts for the height data based on discrete focus positioning. The laser intensity profiles are denoted as (I=Intensity), white LED (visible) images are as (C=color), and the 3D height data are denoted as (H=height). Scanning electron microscopy (SEM) was performed on a Zeiss Sigma VP device (GeminiSEM 500) using the software SmartSEM Version 6.07. The samples were mounted on an aluminum stud using adhesive copper tape and sputter-coated with approximately 6 nm platinum using an Automatic Turbo Coater PLASMATOOL 125 SIN 2020_131 from Ingenieurbüro Peter Liebscher. Cyclic voltammetry (CV) was conducted employing a BioLogic SP-150 as the potentiostat in a voltammetry cell with a three-electrode configuration with an Ag/AgCl reference electrode in acetonitrile, a Pt-wire as the counter electrode, and a Pt working electrode with an inner diameter of 2 mm. The measurements were conducted with different scan rates between 5 and 200 mV s^{-1} in 0.1 M solution with tetrabutylammonium hexafluorophosphate([TBA][PF6]). Ferrocene was used as a calibration agent, and the evaluation proceeded with EC-Lab V11.46. For the inductively coupled plasma mass spectrometry measurements (ICP-MS), a 7500cx ICP-MS (Agilent, Santa Clara, USA) with a CETAC ASX 500 autosampler (Agilent, Santa Clara, USA) was used. 10 mg of particles were reacted with aqua regia for 24 h at 60 °C. The solutions were quantitatively transferred in 50 mL polypropylene (PP) volumetric flasks (BRAND GmbH + CO KG, Wertheim, Germany). Ultrapure water (0.055 μS cm^{-2}) from a PURELAB® Chorus 1 ultrapure water filtration unit (Elga LabWater, High Wycombe, UK) was used to prepare all solutions. From each of these solutions, 50 μL were taken and prepared as 10 mL measurement solutions (dilution factor: 200). A solution containing 10 mg L^{-1} each of Sc (1 g L^{-1} in 5% HNO_3, Alfa®), Y (1 g L^{-1} in 2–3% HNO_3, Merck Certipur®) and Ho (1 g L^{-1} in 2–3% HNO_3, Merck Certipur®) in ultrapure water was prepared as an internal standard solution for all ICP-MS measurements. HNO_3 (69%, ROTIPURAN® Supra, Carl Roth) was used to acidify the measurement solutions. Argon 5.0 (Ar ≥ 99.999 mol%, ALPHAGAZ™ 1 Argon, Air Liquide) was used as plasma gas for ICP-MS measurements. An external calibration was prepared using Co (1 g L^{-1} in 0.005 M HNO_3, Fluka) ICP-MS standard solutions for quantification. For the ICP-MS measurement, a 8900 and a 7500cx ICP-MS (Agilent, Santa Clara, USA) with a CETAC ASX 500 autosampler (Agilent, Santa Clara, USA) was used. Powder X-ray diffraction (PXRD) patterns of the pulverized samples were recorded at room temperature on a D8-A25-Advance diffractometer (Bruker, Karlsruhe, Germany) in Bragg-Brentano θ-θ-geometry (goniometer radius 280 mm) with Cu $K\alpha$-radiation (λ = 154.0596 pm). A 12 μm Ni foil working as a K_β filter and a variable divergence slit were mounted at the primary beam side. A LYNXEYE detector with 192 channels was used at the secondary beam side. Experiments were conducted in a 2θ range of 7 to 120° with a step size of 0.013° and a total scan time of 2 h.

(1) Metallocene Synthesis

One-pot Synthesis of Cobaltocenium Hexafluorophosphate

Sodium cyclopentadienide (**2**): Freshly cut sodium (10.0 g, 435 mmol, 1.00 eq) was added to dry anisole (200 mL) and dicyclopentadiene (60 mL, 443 mmol, 1.02 eq.) in a 1000 mL Schlenk flask with reflux condenser under argon. (Dicyclopentadiene may be solid until 50 °C, warmed in a water bath until it is liquid). The mixture was stirred for 6 h at reflux (T = 154 °C). Here, rotation speeds of 600 + RPM are best for quicker reaction time. If sodium was still present, another 10 mL of dicyclopentadiene was added. After 8 h, the reaction is completed, and the white suspension can be directly used for further synthesis steps.

Bis(cyclopentadienyl)cobalt(III) hexafluorophosphate (**4**): The reaction vessel was cooled to −40 °C, and precooled (0 °C) dry THF (400 mL) was added. After stirring for 15 min at −40 °C, dry $CoBr_2$ (47.0 g, 214 mmol, 0.50 eq.) was added. After reaching room temperature (RT) and stirring for 16 h, the brown solution was oxidized in water (400 mL) by passing air through the solution. After 16 h, the remaining brown solid residue was filtered off. The product was precipitated by sequentially adding KPF_6 (~4×10 g) and filtration after each addition step using a Büchner funnel. Sequential addition was performed until no precipitation was obtained upon KPF_6 addition. The taint precipitate was washed with THF (250 mL) and dried in a vacuum at 40 °C. In some instances, a brown impurity was present, which can be removed by dissolving the crude product in acetonitrile and filtration. The product was obtained as a yellow powder or orange crystals with an overall yield of 52.0 g (155.6 mmol, 71.59%). ^{1}H-NMR (500 MHz, 300 K, CD_3CN, δ in ppm): 4.67 (s, 10-H) (Figure S1).

((Trimethylsilyl)ethynyl)cobaltocenium hexafluorophosphate (**5**): A Schlenk flask with dry THF (1500 mL) and trimethylsilylacetylene (27.7 mL, 194.6 mmol, 1.3 eq) was cooled to −20 °C for 30 min. Next, an *n*-BuLi-solution in hexane (77.8 mL, 2.5 M, 194.6 mmol, 1.3 eq) was slowly added dropwise. After 45 min, solid **4** (50 g, 149.6 mmol, 1.0 eq) was added in one portion. Upon warming to RT, the suspension turns from yellow to dark red, consuming the insoluble starting material **4**. After 2 h, the solution was dried in a vacuum, and the red residue was dissolved in hexane (800 mL) and filtered over anhydrous $MgSO_4$. The solvent was evaporated to obtain a red residue. Dry DCM (600 mL) was added, and the solution was cooled to 0 °C. After 5 min, triphenylcarbenium hexafluorophosphate (75.5 g, 194.6 mmol, 1.3 eq.) was added. After stirring for 30 min at RT, the DCM solution was poured into 2 L *n*-hexane. The solution was filtered via a Büchner funnel and washed with Et_2O (3×250 mL), ice-cold water (2×250 mL), and Et_2O. After drying in a vacuum, **5** is acquired as taint yellow to orange powder with an overall yield of 57.49 g (133.6 mmol, 89.27%). ^{1}H-NMR

(500 MHz, 300 K, CD_3CN, δ in ppm): 0.27 (s, 9-H, *TMS*), 5.66 (s, 5-H, *Cp*), 5.67 (t, 2-H, *CH(Cp1)*), 5.84 (t, 2-H, *CH(Cp2)*) (Figure S2).

Ethynylcobaltocenium hexafluorophosphate (**6**): ((Trimethylsilyl)ethynyl)cobaltocenium hexafluorophosphate (**5**) (29.0 g, 67.4 mmol, 1.0 eq.) was suspended in methanol (400 mL) followed by the addition of KHF_2 (14.5 g, 185.3 mmol, 2.75 eq.). After stirring for 1 h at RT, the solution was filtered, and the solvent was reduced under vacuum to acquire a yellow/green residue. The solid was dissolved in DCM (400 mL) and extracted with saturated KPF_6 aqueous solution (3×100 mL). The DCM phase was dried over $MgSO_4$ and evaporated via a rotary evaporator. Product **6** was found to be a yellow powder with a yield of 75.14% (19.50 g, 50.64 mmol, 93% purity). Here, cobaltocenium PF_6 is present as an impurity (7% by proton NMR) but does not interfere with the following reactions ^{1}H-NMR (500 MHz, 300 K, CD_3CN, δ in ppm): 3.72 (s, 1-H, *Acetylene*), 5.69 (t, 2-H, *CH(Cp1)*), 5.70 (s, 5-H, *Cp*), 5.91 (t, 2-H, *CH(Cp2)*) (Figure S3).

3-(Triethoxysilyl)propan-1-amine ethynyl cobaltocenium PF_6 (**7**): Ethynylcobaltocenium hexafluorophosphate (**6**, 102 mg, 282.3 μmol, 1.0 eq.) was dissolved in dry acetonitrile (2 mL) in a Schlenk tube under argon. 3-(triethoxysilyl)propan-1-amine (APTES) (130 μL, 564.6 μmol, 2.0 eq.) was added to the yellow solution. The solution was stirred at 50 °C for 16 h (after approximately 30 min, a shift from yellow to deep red color could be observed). The conversion was measured by proton NMR with a sample of the raw solution, which was found to be quantitative. The reaction solution was used directly without isolation of the product or purification.^{1}H-NMR (500 MHz, 300 K, CD_3CN, δ in ppm): 0.60 (t, 2-H, *Si-C**H**$_2$-CH$_2$-R*), 1.18 (t, 9-H, *Si-CH$_2$-C**H**$_3$*), 1.63 (qn, 2-H, *Si-CH$_2$-C**H**$_2$-CH$_2$-R*), 3.03 (q, 2-H, *Si-CH$_2$-CH$_2$-C**H**$_2$-R)*,3.79 (t, 6-H, *Si-C**H**$_2$-CH$_3$*), 4.84 (d, 1-H, *N-**H**C=CH-R*), 5.29 (s, 5-H, Cp), 5.46 (pt, 2-H, *CH(Cp1)*), 5.51 (pt, 2-H, *CH(Cp2)*), 7.22 (m, 1-H, *N-HC=C**H**-R*) (Figure S4**).**

(2) Particle Functionalization

OxPart@APTES: hydroxy-rich PSDVB particles (OxPart) (1.00 g) were suspended in toluene (50 mL) in a Schott flask. In the next step, triethylamine (1.38 mL) and 3-(triethoxysilyl) propane-1-amine (APTES) (3.70 mL) were added via syringe, and the mixture was shaken at 600 RPM at 85 °C in a shaking device for 48 h. The particles were filtered and washed via dispersing, centrifugation, and decantation (toluene (3×30 mL), MeOH (2×25 mL) and THF (3×25 mL)). After purification, the product was finally dried in a vacuum at 40 °C, resulting in a yield of 1.232 g.

OxPart@APTES@cobaltocenium PF_6: OxPart@APTES (100 mg) were placed in a 50 mL Schlenk flask. Dry acetonitrile (25 mL) was added, and ethynylcobaltocenium hexafluorophosphate (**7**) (114 mg, 87% purity) was added. The flask was placed in a shaking device at 75 °C and stirred for 65 h. A red color was visible after 12 hours. The particles were purified by centrifugation and redispersion with the following media: acetonitrile (3×40 mL), THF (3×40 mL), and acetone (1×40 mL). The red particular product was finally dried in a vacuum at 40 °C, resulting in a yield of 103 mg.

One-Pot OxPart@APTES-cobaltocenium PF_6: Ethynylcobaltocenium hexafluorophosphate (**7**) (114 mg, 87% purity, 1.0 eq.) was dissolved in dry acetonitrile (15 mL) in a Schott flask. APTES (65 μL, 1.0 eq.) was added, and the yellow solution was shaken at 50 °C and 600 RPM for 24 h. After 30 min, a deep red color could be noticed. In the next step, hydroxy-rich PSDVB particles (OxPart) (100 mg) were added. The solution was shaken at 80 °C for 4 d. The particles were purified using centrifugation-washing steps using ACN, Acetone, and THF. Finally, the particles were dried in a vacuum at 40 °C. The particles were synthesized with varying mass concerning the ethynyl cobaltocenium contents (25, 50, 100, 250 mg) at equal APTES equivalents as well as with varying equivalents of APTES (1, 2, 5, 10 eq.) at fixed 50 mg ethynyl cobaltocenium. For each reaction, the oxidized particle amount was kept at 100 mg.

Supporting Information Summary

Additional proton NMR data of synthesized molecules, SEM and LCMS images, size measurements, cyclic voltammetry of **7**, and EDS and XRD studies of the ceramic material are presented.

Acknowledgements

We want to thank Prof. Dr. Volker Presser for access to the SEM. Instrumentation and technical assistance for this work were provided by the Service Center X-ray Diffraction and the Elemental Analysis group, with financial support from Saarland University and German Science Foundation (project numbers INST 256/349-1 and INST 256/553-1).. We also thank Metrohm for donating the particles. Open Access funding enabled and organized by Projekt DEAL.

Conflict of Interests

The authors declare no conflict of interest.

Data Availability Statement

The data that support the findings of this study are available from the corresponding author upon reasonable request.

Keywords: Cobaltocene · Metallopolymers · Redox-responsiveness · Microparticles · Metallocene

[1] E. Melendez, *Inorg. Chim. Acta* **2012**, *393*, 36–52.
[2] H. B. Gray, Y. S. Sohn, N. Hendrickson, *J. Am. Chem. Soc.* **2002**, *93*, 3603–3612.
[3] M. Atiqullah, M. Tinkl, R. Pfaendner, M. N. Akhtar, I. Hussain, *Polymer Rev.* **2010**, *50*, 178–230.
[4] K. Heinze, H. Lang, *Organometallics* **2013**, *32*, 5623–5625.
[5] G. Roy, R. Gupta, S. Ranjan Sahoo, S. Saha, D. Asthana, P. Chandra Mondal, *Coord. Chem. Rev.* **2022**, *473*, 214816
[6] M. Kasper, K. Sattler, K. Siegmann, U. Matter, H. C. Siegmann, *J. Aerosol Sci.* **1999**, *30*, 217–225.
[7] M. Gallei and J. Elbert in *Recent Advances in Immobilized Ferrocene-Containing* Polymers, (Eds.: J. G. Hardy, F. H. Schacher), The Royal Society of Chemistry, . **2015**, pp. 120–148
[8] B. Fabre, *Acc. Chem. Res.* **2010**, *43*, 1509–1518.
[9] M. Gallei, C. Ruttiger, *Chem. Eur. J.* **2018**, *24*, 10006–10021.
[10] A. S. Abd-El-Aziz, E. A. Strohm, *Polymer* **2012**, *53*, 4879–4921.
[11] A. S. Abd-El-Aziz, C. Agatemor, N. Etkin, *Macromol. Rapid Commun.* **2014**, *35*, 513–559.
[12] D. A. Foucher, B. Z. Tang, I. Manners, *J. Am. Chem. Soc.* **2002**, *114*, 6246–6248.
[13] J. Elbert, M. Gallei, C. Rüttiger, A. Brunsen, H. Didzoleit, B. Stühn, M. Rehahn, *Organometallics* **2013**, *32*, 5873–5878.
[14] R. D. A. Hudson, *J. Organomet. Chem.* **2001**, *637–639*, 47–69.

[15] R. Sun, L. Wang, H. Yu, Z.-U. Abdin, Y. Chen, J. Huang, R. Tong, *Organometallics* **2014**, *33*, 4560–4573.
[16] P. Rohland, E. Schröter, O. Nolte, G. R. Newkome, M. D. Hager, U. S. Schubert, *Progr. Polym. Sci.* **2022**, *125*, 101474
[17] S. M. Beladi-Mousavi, S. Sadaf, A. K. Hennecke, J. Klein, A. M. Mahmood, C. Rüttiger, M. Gallei, F. Fu, E. Fouquet, J. Ruiz, D. Astruc, L. Walder, *Angew. Chem. Int. Ed.* **2021**, *60*, 13554–13558.
[18] Z. Wei, D. Wang, Y. Liu, X. Guo, Y. Zhu, Z. Meng, Z.-Q. Yu, W.-Y. Wong, *J. Mater. Chem. C* **2020**, *8*, 10774–10780.
[19] D. P. Puzzo, A. C. Arsenault, I. Manners, G. A. Ozin, *Angew. Chem. Int. Ed.* **2009**, *48*, 943–947.
[20] A. C. Arsenault, H. Míguez, V. Kitaev, G. A. Ozin, I. Manners, *Adv. Mater.* **2003**, *15*, 503–507.
[21] T. Winter, X. Su, T. A. Hatton, M. Gallei, *Macromol. Rapid Commun.* **2018**, *39*, e1800428.
[22] D. Scheid, C. Lederle, S. Vowinkel, C. G. Schäfer, B. Stühn, M. Gallei, *J. Mater. Chem. C* **2014**, *2*, 2583
[23] S. Schöttner, R. Hossain, C. Rüttiger, M. Gallei, *Polymers* **2017**, *9*, 491
[24] J. Elbert, F. Krohm, C. Rüttiger, S. Kienle, H. Didzoleit, B. N. Balzer, T. Hugel, B. Stühn, M. Gallei, A. Brunsen, *Adv. Funct. Mater.* **2014**, *24*, 1493–1493.
[25] R. H. Staff, M. Gallei, M. Mazurowski, M. Rehahn, R. Berger, K. Landfester, D. Crespy, *ACS Nano* **2012**, *6*, 9042–9049.
[26] X. Liu, A. Rapakousiou, C. Deraedt, R. Ciganda, Y. Wang, J. Ruiz, H. Gu, D. Astruc, *Chem. Commun.* **2020**, *56*, 11374–11385.
[27] F. Liu, T. Abdiryim, X. Liu, *Polymer* **2024**, *305*, 127170.
[28] J. P. Hurvois, C. Moinet, *J. Organomet. Chem.* **2005**, *690*, 1829–1839.
[29] E. V. Leonova, N. S. Kochetkova, *Rus. Chem. Rev.* **1973**, *42*, 278–292.
[30] F. Fu, R. Ciganda, Q. Wang, A. Tabey, C. Wang, A. Escobar, A. M. Martinez-Villacorta, R. Hernández, S. Moya, E. Fouquet, J. Ruiz, D. Astruc, *ACS Catalysis* **2018**, *8*, 8100–8106.
[31] M. V. Kharlamova, C. Kramberger, *Nanomater.* **2021**, *11*, 2984
[32] B. Wang, Y. Zhuang, X. Luo, S. Xu, X. Zhou, *Macromolecules* **2003**, *36*, 9684–9686.
[33] R. S. Stojanovic, A. M. Bond, *Anal. Chem.* **2002**, *65*, 56–64.
[34] L. Zhao, X. Liu, L. Zhang, G. Qiu, D. Astruc, H. Gu, *Coord. Chem. Rev.* **2017**, *337*, 34–79.
[35] H. Gu, R. Ciganda, P. Castel, S. Moya, R. Hernandez, J. Ruiz, D. Astruc, *Angew. Chem. Int. Ed.* **2018**, *57*, 2204–2208.
[36] A. Feuerstein, B. Bossmann, T. Rittner, R. Leiner, O. Janka, M. Gallei, A. Schäfer, *ACS Macro Lett.* **2023**, *12*, 1019–1024.
[37] H. Li, P. Yang, J. Hwang, P. Pageni, A. W. Decho, C. Tang, *Biomater. Transl.* **2022**, *3*, 162–171.
[38] J. Hwang, Y. Cha, L. Ramos, T. Zhu, L. Buzoglu Kurnaz, C. Tang, *Chem. Mater.* **2022**, *34*, 5663–5672.
[39] D. Astruc, F. Lu, J. R. Aranzaes, *Angew. Chem. Int. Ed.* **2005**, *44*, 7852–7872.
[40] J. E. Sheats, M. D. Rausch, *J. Org. Chem.* **1970**, *35*, 3245–3249.
[41] S. Vanicek, H. Kopacka, K. Wurst, T. Müller, H. Schottenberger, B. Bildstein, *Organometallics* **2014**, *33*, 1152–1156.
[42] Y. Wang, A. Rapakousiou, C. Latouche, J. C. Daran, A. Singh, I. Ledoux-Rak, J. Ruiz, J. Y. Saillard, D. Astruc, *Chem. Commun.* **2013**, *49*, 5862–5864.
[43] A. Seubert, J. S. Tripp, R. Aeschlimann, O. Michael, *Verfahren zur Erzeugung einer hydrophilen Oberfläche auf PS/DVB Copolymerpartikeln. EP3953034 A1* **2020**.
[44] D. Schmitt, O. Janka, R. Leiner, G. Kickelbick, M. Gallei, *Mater. Adv.* **2024**, *5*, 3037-3050.
[45] D. Schmitt, A. Schiesser, M. Gallei, *ACS Appl. Polym. Mater.* **2024**, *6*, 2993–3002.
[46] A. Y. Fadeev, T. J. McCarthy, *Langmuir* **2000**, *16*, 7268–7274.
[47] S. Gauthier, J. P. Aimé, T. Bouhacina, A. J. Attias, B. Desbat, *Langmuir* **1996**, *12*, 5126–5137.
[48] T. Gutmann, B. Kumari, L. Zhao, H. Breitzke, S. Schoettner, C. Ruettiger, M. Gallei, *J. Phys. Chem. C* **2017**, *121*, 3896–3903.
[49] R. M. Pasternack, S. Rivillon Amy, Y. J. Chabal, *Langmuir* **2008**, *24*, 12963–12971.
[50] N. Rozlosnik, M. C. Gerstenberg, N. B. Larsen, *Langmuir* **2003**, *19*, 1182–1188.
[51] E. T. Vandenberg, L. Bertilsson, B. Liedberg, K. Uvdal, R. Erlandsson, H. Elwing, I. Lundström, *J. Coll. Interf. Sci.* **1991**, *147*, 103–118.
[52] K. Wen, R. Maoz, H. Cohen, J. Sagiv, A. Gibaud, A. Desert, B. M. Ocko, *ACS Nano* **2008**, *2*, 579–599.
[53] D. K. Bhowmick, S. Linden, A. Devaux, L. De Cola, H. Zacharias, *Small* **2012**, *8*, 592–601, 619.
[54] M. Briesenick, M. Gallei, G. Kickelbick, *Macromolecules* **2022**, *55*, 4675–4691.
[55] G. Mera, M. Gallei, S. Bernard, E. Ionescu, *Nanomaterials* **2015**, *5*, 468–540.
[56] M. Natali, J. M. Kenny, L. Torre, *Progr. Mater. Sci.* **2016**, *84*, 192–275.
[57] L. Xu, L. Liang, C. Chen, Z.-H. Chen, Z.-B. Lv, M.-L. Fu, B. Yuan, *J. Environ. Chem. Eng.* **2023**, *11*, 111605.
[58] N. Zhang, Z. Xu, W. Deng, X. Wang, *Electrochem. Energy Rev.* **2022**, *5*.
[59] I. Luisetto, F. Pepe, E. Bemporad, *J. Nanopart. Res.* **2008**, *10*, 59–67.
[60] S. Iravani, R. S. Varma, *Green Chem.* **2020**, *22*, 2643–2661.
[61] M. Li, S. A. Odom, A. R. Pancoast, L. A. Robertson, T. P. Vaid, G. Agarwal, H. A. Doan, Y. L. Wang, T. M. Suduwella, S. R. Bheemireddy, R. H. Ewoldt, R. S. Assary, L. Zhang, M. S. Sigman, S. D. Minteer, *ACS Energy Lett.* **2021**, *6*, 3932–3943.

Manuscript received: June 18, 2024
Accepted manuscript online: July 29, 2024
Version of record online: September 19, 2024